# The Structure of Chaotic Magnetic Field Lines in a Tokamak with External Nonsymmetric Magnetic Perturbations

Elton César da Silva, Iberê Luiz Caldas, and Ricardo Luiz Viana

***Abstract*—We consider the effects of external nonsymmetric magnetostatic perturbations caused by resonant helical windings and a chaotic magnetic limiter on the plasma confined in a tokamak. The main purpose of both types of perturbation is to create a region in which field lines are chaotic in the Lagrangian sense: two initially nearby field lines diverge exponentially through many turns around the tokamak. The equilibrium field is obtained from the equations of magneto-hydrodynamic equilibrium written down in a polar toroidal coordinate system. The magnetic fields generated by the resonant helical windings and the chaotic magnetic limiter are obtained through an analytical solution of Laplace equation. The magnetic field line equations are integrated to give a Hamiltonian mapping of field lines that we use to characterize the structure of chaotic field lines. In the case of resonant windings, we obtained the map by both numerical integration and a Hamiltonian formulation. For a chaotic limiter, we analytically derived a symplectic map by using a Hamiltonian formulation.**

***Index Terms*—Chaotic magnetic limiter, Hamiltonian formulation for field line flow, magnetic field line mapping, magnetic perturbations in tokamaks, resonant helical windings.**

## I. Introduction

FUSION PLASMA machines are based in some magnetic confinement scheme. Among the various schemes devised for fusion applications, the tokamak is one of the most promising candidates to achieve this goal. Tokamaks are basically toroidal pinches in which a plasma column is formed by ohmic heating of a low-pressure filling gas, produced by electric fields generated in pulses by transformer coils. The plasma torus is then confined by the superposition of two basic fields: 1) a toroidal magnetic field produced by pick-up coils mounted around the tokamak, and 2) a poloidal field generated by the plasma column itself [1]. The combination of these fields results in helical magnetic field lines. From a geometrical point of view, it is convenient to view these field lines as lying on nested toroidal surfaces, called magnetic surfaces, on which the gradient of pressure that causes the plasma expansion is counterbalanced by the Lorentz force that appears due to the interaction between the plasma current and the magnetic field, in an equilibrium configuration [2].

A Hamiltonian approach to this situation consists of a parameterization of the field lines by means of a spatial ignorable coordinate. With respect to this coordinate, the equilibrium configuration must exhibit a symmetry. This parameter plays the role of time in the Hamilton canonical equations, the other variables being field line coordinates and/or magnetic surface labels as well [3]. One of the advantages of this approach is the possibility of describing field lines by means of Hamiltonian maps, reducing the number of degrees of the system [4]. In this framework, symmetry-breaking magnetic field perturbations alter this behavior, and field lines may become chaotic in a lagrangean sense: two initially nearby field lines diverge exponentially through many turns around a toroidal system [5], [6].

A context in which the existence of chaotic magnetic field lines has profound implications for the plasma confinement in tokamaks is the control of the plasma-wall interactions. They occur frequently as a result of collisions of particles—which escape from the plasma and cross the vacuum region that surrounds it—with the tokamak inner metallic wall [1]. One of the technological problems in the operation of tokamaks turns to be the control of these plasma-wall interactions [7]. The confinement quality is affected by the presence of impurities released from the inner wall due to sputtering processes caused by localized energy and particle loadings. Controlling this interaction leads to a decrease of the impurity content in the plasma core and improves plasma confinement.

As an example, plasmas in modern tokamaks and Stellarators are bounded by a separatrix between closed field lines on toroidal magnetic surfaces and open field lines that direct plasma particles from the plasma edge to divertor plates [8], [9]. In this arrangement, the diverted plasma particles can be recycled and pumped in order to reduce impurity levels in the plasma. In an ideal tokamak, the separatrix is a sharp surface, but asymmetries in the equilibrium field create a layer of chaotic field lines between the last confining surface and the separatrix [10], [11]. Another type of ergodic divertor uses a region of chaotic field lines in the plasma edge. Open field lines that hit the divertor plates guide plasma particles to the wall [5]. Both divertor concepts aim to control anomalous plasma edge transport and improve the confinement quality. Since a nonsymmetric magnetic field configuration may be described as a one and a half degree of freedom Hamiltonian system, the

Manuscript received January 2, 2001; revised April 17, 2001. This work was supported in part by the following Brazilian government agencies: CNPq, CAPES, FAPESP, and Fundação Araucária (State of Paraná).

E. C. da Silva and I. L. Caldas are with the Instituto de Física, Universidade de São Paulo, São Paulo 05315-970, SP, Brazil (e-mail: ecesar@uol.com.br; ibere@if.usp.br).

R. L. Viana is with the Departamento de Física, Universidade Federal do Paraná, Curitiba 81531-990, PR, Brazil (e-mail: viana@fisica.ufpr.br).

Publisher Item Identifier S 0093-3813(01)07210-1.

field line behavior due to an ergodic divertor is near-integrable, and has been intensively studied by means of Hamiltonian maps in tokamaks [5], [12], as well as in Stellarators [13].

Like an ergodic divertor, a chaotic magnetic limiter (CML) creates a "cold" boundary layer of chaotic magnetic field lines in the peripheral region of the tokamak [14]. It has been argued that suitably applied chaotic magnetic fields can enhance heat and particle diffusion in this peripheral region of the tokamak vessel, so as to uniformize these loadings on the metallic wall [15], [7]. A design for the CML consists of one or more grid-shaped coils of finite width and wound around the torus, each of them with wires that conduct electrical currents in opposite senses for adjacent segments. The magnetic field generated by such configuration falls down rapidly with the distance from the wall, and can interact with the equilibrium magnetic field in order to create chains of magnetic islands in the peripheral region of the torus.

Another scenario where chaotic field lines play a role in the plasma behavior is the case of disruptive instabilities. Severe obstructions to the obtention of long lasting plasma confinement in fusion devices are the existence of instabilities and anomalous particle transport. An experimental method to artificially produce this chaotic region is the use of conductors wound externally around the device vessel wall in a suitable way [16]–[18]. An example is provided by resonant helical windings (RHW), which are helical coils that create resonant magnetic perturbation inside the plasma. Disruptive instabilities in tokamaks are typically preceded by Mirnov oscillations, which are fluctuations of the poloidal magnetic field that can be detected by magnetic probes [19]. The use of RHW has been proved to inhibit these oscillations below a threshold value of the perturbation [17], [20], [21]. An RHW creates a magnetic island structure within the plasma column that hinders a rotation of the magnetohydrodynamical (MHD) modes. Magnetic islands are field line structures of tubular shape that wind around the torus. A cross section of these islands reveals a phase portrait (in Hamiltonian maps) very similar to pendulum trajectories in phase space [22].

Minor, or soft disruptions can occur within the plasma in the region comprising the main island and its satellites, leading eventually to the loss of confinement. The creation of a thick layer of chaotic magnetic field lines in this region is responsible for these minor disruptions [16], [17], [23]. The onset of chaotic behavior of magnetic field lines in a tokamak with RHW has been studied by several authors [24]–[26]. The origin of chaotic field lines is the interaction between magnetic islands produced by the perturbing field on the equilibrium structure. An RHW would cause destruction of part of the equilibrium magnetic surfaces if toroidal effects are taken into account, and if the perturbation is strong enough [25].

Since the action of either an RHW, an ergodic divertor, or a CML, is a symmetry-breaking perturbation of the equilibrium magnetic configuration, the magnetic islands that appear in the plasma due to their operation are expected to have a thin region of chaotic field lines attached to the neighborhood of their separatrices [22]. The generation of a thick chaotic region, essential to the RHW or CML action, can be achieved by means of the interaction between adjacent island chains. In the CML case, due to the fast radial decrease of the perturbation field, only the peripheral islands have a significant width. Therefore, the inner region of the plasma column is not supposed to be noticeably affected by a CML.

A theoretical description for the CML, using this conceptual background, was pioneered by Martin and Taylor, who have proposed a model in which the magnetic field line behavior is described by a map [27]. This map has been later improved by the addition of toroidicity effects, and considering a design for the CML rings that reflects the actual paths followed by field lines [28]. Hamiltonian descriptions for field line behavior have been recently proposed for the CML [29], RHW [30], and ergodic divertor [5].

An efficient design for an RHW or a CML depends on an adequate choice of equilibrium and perturbing magnetic fields, as well as a convenient coordinate system that evidences the resonant effects [31]. Following a large number of field lines through numerical integration of their differential equation typically requires a considerably large computer time, and is a rather unsatisfactory way to determine how chaotic field lines behave when model parameters are changed. To answer this and other related questions, we would benefit from an analytically obtained map for field lines. Early studies used the well-known Chirikov–Taylor standard map [32], however this and other related twist maps may not be appropriate to model some other features of field line behavior. Simple analytical maps were introduced to describe separatrix chaos in a single-null [11] and ergodic divertor [12]. Balescu *et al.* have proposed a general class of Hamiltonian maps to describe a wide variety of field line configurations [4], [33].

In this paper, we will describe in some detail how the equilibrium and nonsymmetric perturbing magnetic fields are obtained, and how a Hamiltonian map can be derived by using these model fields. For an RHW, we have obtained this map numerically. Phase portraits are shown in order to evidence the creation of a chaotic field line region. For a CML, we were able to obtain analytically the map, by using as a tool a Hamiltonian formulation for field line flow. The methods here exposed, however, are not restricted to the specific models we use and may be adapted to consider other related situations in which there is an external magnetic perturbation, like error fields.

The toroidicity of the equilibrium plasma configuration puts some restrictions on the use of common toroidal coordinates, since it is desirable that coordinate surfaces should coincide as much as possible with actual magnetic surfaces of the equilibrium field. A coordinate system devised to deal with this problem was proposed by Kucinski and Caldas [34]. The tokamak equilibrium field will be obtained as an approximate analytical solution, in this coordinate system, of an elliptic partial differential equation for the poloidal magnetic flux, in an ideal MHD equilibrium theory. The perturbing EML fields will be obtained through an explicit solution of the Laplace equation, supposing they are vacuum fields. The total magnetic field will be the superposition of these fields, which is justifiable when the plasma response is negligible. This turns to be the case in the majority of situations, except for states of marginal stability, that are not considered in this work.

This paper is organized as follows: in Section II, we present the equilibrium magnetic field calculation by solving the corre-

sponding MHD equilibrium equation. Section III is devoted to the obtention of the perturbing magnetic field due to an RHW, showing numerically obtained maps. In Section IV, we derive the magnetic field due to a CML, and show how to build an analytical area-preserving map for field lines. The last section is left for our conclusions. An Appendix is included on the coordinate system used in this work.

## II. Tokamak Equilibrium Magnetic Field

We suppose that the tokamak plasma is in a state of static MHD equilibrium. By using the ideal MHD equations, we have that [2]

$$\mathbf{J}_0 \times \mathbf{B}_0 = \nabla p_0 \tag{1}$$

where

$\mathbf{J}_0$ plasma equilibrium electric current density;
$\mathbf{B}_0$ magnetic field;
$p_0$ kinetic pressure.

Taking the dot product of (1) with $\mathbf{B}_0$ results in

$$\mathbf{B}_0.\nabla p_0 = 0 \tag{2}$$

such that the equilibrium magnetic field lines lie on constant pressure surfaces with topology of nested tori, known as *magnetic surfaces*.

Instead of the pressure, we may label these surfaces with other surface quantities, like the poloidal magnetic flux $\Psi_p$, defined as the flux of $\mathbf{B}_0$ through a ribbon from the magnetic axis to a coordinate curve. In this way, we may rewrite (2) in the form

$$\mathbf{B}_0.\nabla \Psi_p = 0. \tag{3}$$

Equations (1) and (3) show that all points of a magnetic surface the plasma pressure must be counterbalanced by the Lorentz force. The existence of magnetic surfaces may be regarded as a necessary, albeit not sufficient, condition for plasma confinement. In addition, to present closed magnetic surfaces the system must have some spatial symmetry.

There are many coordinate systems to describe magnetic field lines in a tokamak [35], its choice being dictated by the symmetries exhibited by the system. For the so-called local coordinates $(r, \theta, \varphi)$ that are a kind of cylindrical coordinates with toroidal curvature, the coordinate surfaces $r =$ const. hardly coincide with actual equilibrium magnetic surfaces. A better choice would be the toroidal coordinates $(\xi, \omega, \varphi)$, but their coordinate surfaces are not suitable as well. We have used in this paper a polar toroidal coordinate system $(r_t, \theta_t, \varphi_t)$ [34] which, in the large aspect ratio limit, reduces to the local system. Further details about these coordinate systems are found in the Appendix.

Consider a field line in a tokamak where $R_0'$ denotes the radius of the magnetic axis, that is shifted with respect to the geometric major $(R_0)$ due to a toroidicity effect (Shafranov shift). The tokamak minor radius is denoted by $b_t$. The spatial symmetry is with respect to the azimuthal angle $\varphi$, and the magnetic surface labels depend only on the remaining coordinates, as the poloidal flux $\Psi_p = \Psi_p(r_t, \theta_t)$. The MHD equations may be used to derive an elliptic partial differential equation for the equilibrium poloidal magnetic flux, which bears the names of Grad, Shafranov, and Schlüter, who have derived it in the late 1950s [2]. The corresponding equation in the polar toroidal system is [36]

$$\begin{aligned}\frac{1}{r_t}\frac{\partial}{\partial r_t}\left(r_t\frac{\partial \Psi_p}{\partial r_t}\right)+\frac{1}{r_t^2}\frac{\partial^2 \Psi_p}{\partial \theta_t^2}&\\ = \mu_0 J_{30}(\Psi_p)+\mu_0 {R_0'}^2\frac{dp_0}{d\Psi_p}\left(2\frac{r_t}{R_0'}\cos\theta_t+\frac{r_t^2}{{R_0'}^2}\sin^2\theta_t\right)&\\ +\frac{r_t}{R_0'}\left[\cos\theta_t\left(2\frac{\partial^2\Psi_p}{\partial r_t^2}+\frac{1}{r_t}\frac{\partial\Psi_p}{\partial r_t}\right)\right.&\\ \left.+\sin\theta_t\left(\frac{1}{r_t^2}\frac{\partial\Psi_p}{\partial\theta_t}-\frac{2}{r_t}\frac{\partial^2\Psi_p}{\partial\theta_t\partial r_t}\right)\right]&\end{aligned} \tag{4}$$

where $J_{30}$ is the toroidal component of the equilibrium plasma current density, given by

$$J_{30}(\Psi_p) = -{R_0'}^2\frac{dp_0}{d\Psi_p} - \frac{d}{d\Psi_p}\left(\frac{1}{2}\mu_0 I^2\right) \tag{5}$$

where $I = I(r_t, \theta_t)$ is the poloidal current function, that is the current density flux through the same surface used in the definition of $\Psi_p$.

The equilibrium magnetic field contravariant components, in terms of the surface functions $\Psi_p$ and $I$, are

$$B_0^1 = -\frac{1}{R_0' r_t}\frac{\partial\Psi_p}{\partial\theta_t} \tag{6}$$

$$B_0^2 = \frac{1}{R_0' r_t}\frac{\partial\Psi_p}{\partial r_t} \tag{7}$$

$$B_0^3 = -\frac{\mu_0 I}{R^2} \tag{8}$$

where

$$R^2 = {R_0'}^2\left[1-2\left(\frac{r_t}{R_0'}\right)\cos\theta_t-\left(\frac{r_t}{R_0'}\right)^2\sin^2\theta_t\right]. \tag{9}$$

Closed form solutions to the Grad–Schlüter–Shafranov equation are relatively rare, especially in the coordinate system used here. Hence, we will look for an approximate solution

$$\Psi_p(r_t, \theta_t) = \Psi_{p0}(r_t) + \delta\Psi_p(r_t, \theta_t) \tag{10}$$

where $|\delta\Psi_p| \ll |\Psi_{p0}|$. We expand $J_{30}$ and $dp_0/d\Psi_p$ in powers of $\delta\Psi_p$ and retain first-order terms only. In the large aspect ratio limit $(R_0' \gg b_t)$, and supposing that in lowest order the solution $\Psi_{p0}$ does not depend on $\theta_t$, (4) reduces to the equilibrium equation in a cylindrical geometry. The intersections of magnetic surfaces $\Psi_{p0}(r_t) =$ const. with a toroidal plane $\varphi = 0$ are not concentrical circles, but present a Shafranov shift toward the exterior equatorial region.

To solve (4), we need to assume spatial profiles for both the pressure $p$ and current function $I$. In lowest order, however, it is sufficient to assume a single profile for the toroidal current density $J_{30}$, as given by (5) in terms of $p$ and $I$. So, we choose

a peaked current profile, commonly observed in tokamak discharges [2], and given by

$$J_{30}(r_t) = \frac{I_p R_0'}{\pi a^2}(\gamma+1)\left(1-\frac{r_t^2}{a^2}\right)^{\gamma} \tag{11}$$

where

| | |
|---|---|
| $I_p$ | total plasma current; |
| $a(<b_t)$ | plasma column radius; |
| $\gamma$ | positive constant. |

This results in

$$\Psi_p(r_t,\,\theta_t) = \Psi_{p0}(r_t) + \frac{d\Psi_{p0}}{dr_t}\cos\theta_t \int_{r_t}^{a} \frac{\chi}{R_0'}\Lambda(\chi)\,d\chi \tag{12}$$

where

$$\Psi_{p0}(r_t) = \frac{\mu_0 I_p R_0'}{4\pi}\sum_{j=1}^{\gamma+1}\frac{1}{j}\left[1-\left(1-\frac{r_t^2}{a^2}\right)^{j}\right] \tag{13}$$

and

$$\Lambda(r_t) = \beta_p - 1 + \left(r_t\frac{d\Psi_{p0}}{dr_t}\right)^{-2}\int_0^{r_t}\chi\left(\frac{d\Psi_{p0}}{d\chi}\right)^2 d\chi \tag{14}$$

where $\beta_p$ is the dimensionless ratio between kinetic and magnetic pressures. It turns out that $\Lambda(r_t = a)$ is an asymmetry factor for the poloidal magnetic field, given by

$$\Lambda(a) = \tfrac{1}{2}\,\ell_i + \beta_p - 1, \tag{15}$$

where $\ell_i$ is the normalized internal plasma inductance by unit length [1].

In lowest order, we have found the following (contravariant) equilibrium magnetic field components

$$B_0^1 = 0 \tag{16}$$

$$B_0^2 = \frac{\mu_0 I_p}{2\pi r_t^2}\left[1-\left(1-\frac{r_t^2}{a^2}\right)^{\gamma+1}\right] \tag{17}$$

$$B_0^3 = \frac{\mu_0 I_e}{2\pi {R_0'}^2}\left(1-2\frac{r_t}{R_0'}\cos\theta_t\right)^{-1} \tag{18}$$

where $I_e$ is the external current that generates the equilibrium toroidal field. It is related to the poloidal current function $I$ in (5) by

$$I = -\frac{I_e}{2\pi}\left\{1+(1-\beta_p)(\gamma+1)\left(\frac{I_p R_0'}{I_e a}\right)^2\sum_{j=\gamma+1}^{2\gamma+1}\cdot\frac{1}{j}\left(1-\frac{r_t^2}{a^2}\right)^{j}\right\} \tag{19}$$

which gives $I \approx -I_e/2\pi$ for large aspect ratio.

Magnetic field lines of the equilibrium field spiral on magnetic surfaces $\Psi_p = \text{const}$. Their helical paths are described by the so-called *safety factor* $q = q(r_t,\,\theta_t)$, that gives the average poloidal angle swept by the field line after one complete toroidal turn. Consider the differential equations for the field lines in polar toroidal coordinates

$$\frac{dr_t}{B_0^1(r_t,\,\theta_t)} = \frac{d\theta_t}{B_0^2(r_t,\,\theta_t)} = \frac{d\varphi_t}{B_0^3(r_t,\,\theta_t)}. \tag{20}$$

The poloidally averaged safety factor is given by [1]

$$q(r_t) = \frac{1}{2\pi}\int_0^{2\pi}\left(\frac{d\varphi_t}{d\theta_t}\right)d\theta_t = \frac{1}{2\pi}\int_0^{2\pi}\frac{B_0^3(r_t,\,\theta_t)}{B_0^2(r_t,\,\theta_t)}\,d\theta_t. \tag{21}$$

Using (17) and (18) in (21), results in

$$q = q_c(r_t)\left(1-4\frac{r_t^2}{{R_0'}^2}\right)^{-1/2} \tag{22}$$

where

$$q_c(r_t) = \frac{I_e}{I_p}\frac{r_t^2}{{R_0'}^2}\left[1-\left(1-\frac{r_t^2}{a^2}\right)^{\gamma+1}\right]^{-1}. \tag{23}$$

In the following, we will choose $q \approx 1$ at the magnetic axis and $q \approx 5$ at plasma edge ($r_t = a$). We also normalize lengths to the minor radius ($b_t = 1$) and choose parameters so that $a/R_0' = 0.26$ and $\gamma = 3$, which are values typical for tokamak discharges [21], [18].

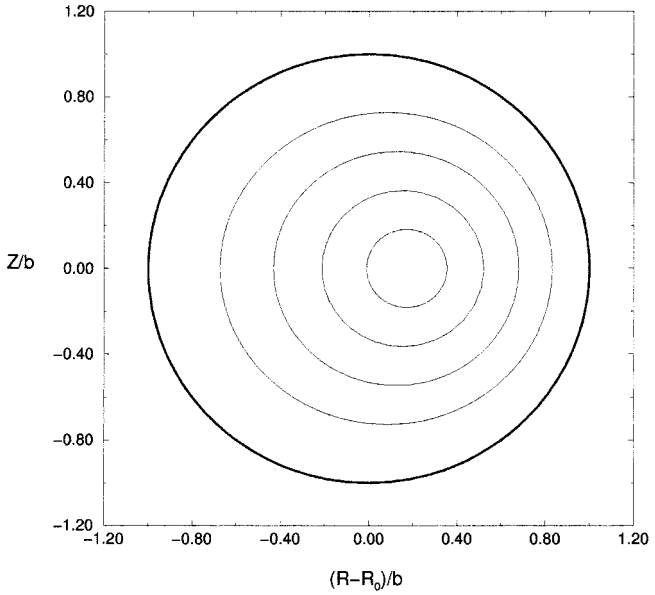


Fig. 1. Cross section (at $\varphi = 0$) of some equilibrium magnetic surfaces of a tokamak plasma, with $b_t/R_0 = 0.36$, $\gamma = 3.0$ and $q \approx 1$ at the magnetic axis.

In Fig. 1, we show, in a surface of section $\varphi = 0$, magnetic surfaces for the equilibrium field. The magnetic surfaces are nested tori, and we may see a Shafranov shift of the magnetic axis (which is a degenerate zero-volume torus at $R_0'$) with respect to the geometric axis at the origin (at $R = R_0$), which appears due to the toroidal geometry [2]. Since the zeroth- and first-order results practically coincide, we will use in this work only the zeroth-order flux $\Psi_{p0}(r_t)$. Fig. 2 presents radial profiles for the poloidal [Fig. 2(a)] and toroidal [Fig. 2(b)] equilibrium field components, using the same parameters as in Fig. 1, as well the corresponding safety factor parabolic profile [Fig. 2(c)]. The poloidal field component is roughly symmetric with respect to the geometric axis, and the corresponding asymmetry factor $\Lambda(a)$ is not very large. The

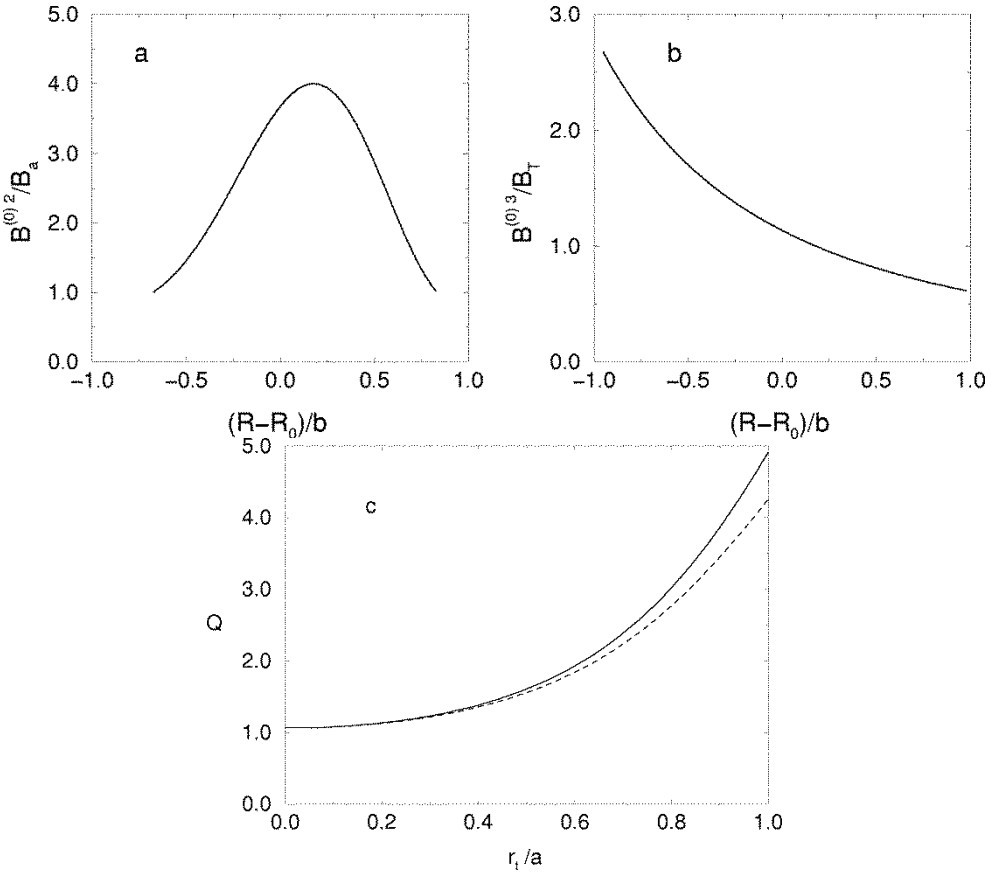


Fig. 2. Radial profiles for: (a) normalized poloidal equilibrium field; (b) normalized toroidal equilibrium field; (c) safety factor of a tokamak. In (c), we show both the zeroth-(dashed line) and first-order (full line) results. Tokamak parameters are the same as in Fig. 1.

toroidal component is stronger in the internal part of the torus, since the coils that generate it are more densely packed there. Fig. 2(c) shows two safety factor profiles, calculated by taking into account or neglecting first order corrections. Both have considered the toroidal geometry; the difference is noticeable only at the plasma edge and results in a slight magnetic surface displacement.

## III. Perturbing Magnetic Field Due to Resonant Helical Windings

It has been conjectured that disruptive instabilities may result from topological changes in the magnetic surface with safety factor $q = 2 : 1$ [17]. An RHW may be used to produce a resonant external perturbation with suitably chosen mode numbers, in order to investigate the onset of this instability and how it could be controlled. The use of RHW with other mode numbers may control topological changes on other rational magnetic surfaces, like those with $q = 3 : 2$ [16] and $q = 4 : 1$ [21]. In Fig. 3, we present a scheme for an RHW with mode numbers $m_0 = 4$ and $n_0 = 1$, consisting of a pair of thin wires conducting a current $I_h$ (in opposite senses for each conductor), wound around the tokamak wall at $r_t = b_t$. A $(4, 1)$ helical coil closes on itself after four turns along the toroidal direction and one turn along the poloidal direction. The design of an RHW needs to take into account the effects of the toroidal geometry. While in a cylindrical approximation the helical pitch is constant, adding toroidicity we find that the pitch is not uniform due to the behavior of the toroidal field component, which is stronger in the inner part of the torus [see Fig. 2(b)].

Hence, we use a winding law to best emulate the actual paths followed by magnetic field lines, introducing a tunable parameter $\lambda$, such that the variable

$$u_t = m_0(\theta_t + \lambda \sin \theta_t) - n_0\varphi_t \tag{24}$$

is constant along a given helical winding [28]. We consider a pair of RHWs, located at $u_t = 0$ and $u_t = \pi$, respectively. In the next section we will see how to choose an appropriate value for $\lambda$, taken into account the resonant perturbation to be excited.

Since the penetration time of the metallic tokamak wall is very short (tens of microseconds for typical millisecond plasma discharges), we will neglect its role in the obtention of the magnetic field $\mathbf{B}_h$ generated by an RHW, described by the singular surface current density

$$\mathbf{J}_h(r_t, \theta_t) = \frac{I_h}{R_0' r_t}\, \delta(r_t - b_t)[\delta(u_t) - \delta(u_t - \pi)]\hat{e}_{u_t} \tag{25}$$

where $\hat{e}_{u_t}$ is the basis vector corresponding to the angle given by (24) (see Fig. 3). The boundary condition to be applied at the wall $r_t = b_t$ is

$$\mathbf{B}_h^{ext} - \mathbf{B}_h^{int} = -\mu_0 \int_i^e d\mathbf{r}_n \times \mathbf{J}_h \tag{26}$$

where

$$d\mathbf{r}_n = \left(1 - 2\,\frac{r_t}{R_0'}\cos\theta_t\right)^{-1} dr_t \hat{e}^1. \tag{27}$$

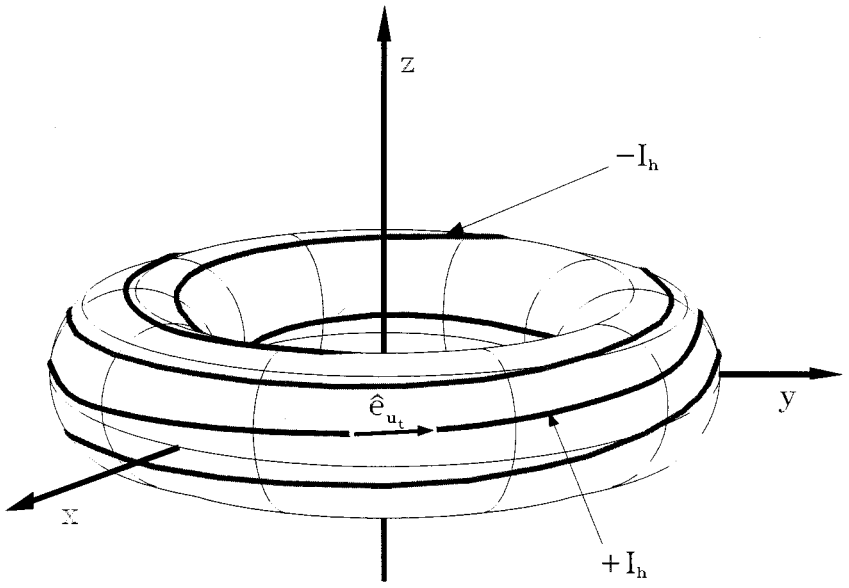


Fig. 3. Scheme of a pair of resonant helical windings with $(m_0,\ n_0) = (4,\ 1)$ in a tokamak.

Neglecting the plasma response to the field generated by an RHW, it may be considered a vacuum field, so that it is given by $\mathbf{B}_h = \nabla\Phi_M$, where $\Phi_M = \Phi_M(r_t,\ \theta_t,\ \varphi_t)$ is a magnetic scalar potential satisfying Laplace equation. In the polar toroidal coordinate system used here it reads

$$\nabla^2\Phi_M = \frac{1}{r_t}\frac{\partial}{\partial r_t}\left(r_t\frac{\partial\Phi_M}{\partial r_t}\right) + \frac{1}{r_t^2}\frac{\partial^2\Phi_M}{\partial\theta_t^2} - \left(\frac{r_t}{R_0'}\right) \cdot\left\{\cos\theta_t\left[2\frac{\partial^2\Phi_M}{\partial r_t^2} + \frac{3}{r_t}\frac{\partial\Phi_M}{\partial r_t}\right] - \sin\theta_t\left[\frac{1}{r_t^2}\frac{\partial\Phi_M}{\partial\theta_t} + \frac{2}{r_t}\frac{\partial^2\Phi_M}{\partial\theta_t\partial r_t}\right]\right\} + \frac{1}{R^2}\frac{\partial^2\Phi_M}{\partial\varphi_t^2} = 0 \tag{28}$$

which may be formally written as an expansion in powers of the inverse aspect ratio $b_t/R_0'$

$$\mathcal{L}_0(\Phi_M) + \left(\frac{b_t}{R_0'}\right)\mathcal{L}_1(\Phi_M) + \left(\frac{b_t}{R_0'}\right)^2\mathcal{L}_2(\Phi_M) + \cdots = 0 \tag{29}$$

where we defined the differential operators

$$\mathcal{L}_0(\,) \equiv \rho\frac{\partial}{\partial\rho}\left(\rho\frac{\partial}{\partial\rho}\right) + \frac{\partial^2}{\partial\theta_t^2} \tag{30}$$

$$\mathcal{L}_1(\,) \equiv -\rho\left\{\cos\theta_t\left[2\rho^2\frac{\partial^2}{\partial\rho^2} + 3\rho\frac{\partial}{\partial\rho}\right] - \sin\theta_t\left[\frac{\partial}{\partial\theta_t} + 2\rho\frac{\partial^2}{\partial\theta_t\partial\rho}\right]\right\} \tag{31}$$

$$\mathcal{L}_2(\,) \equiv \rho^2\frac{\partial^2}{\partial\varphi_t^2} \tag{32}$$

with $\rho \equiv r_t/b_t$.

Likewise, we may expand the magnetic scalar potential as

$$\Phi_M = \Phi_M^{(0)} + \left(\frac{b_t}{R_0'}\right)\Phi_M^{(1)} + \left(\frac{b_t}{R_0'}\right)^2\Phi_M^{(2)} + \cdots \tag{33}$$

so that, up to first-order terms, the scalar potential is given by the following coupled system of partial differential equations

$$\mathcal{L}_0\left(\Phi_M^{(0)}\right) = 0, \tag{34}$$

$$\mathcal{L}_0\left(\Phi_M^{(1)}\right) = -\mathcal{L}_1\left(\Phi_M^{(0)}\right). \tag{35}$$

The general solution of (34) is known to be [37]

$$\Phi_M^{(0)}(\rho,\ \theta_t,\ \varphi_t) = \sum_{N=1}^{\infty}\sum_{k=-\infty}^{\infty} c_{N,k}^{(0)}\mathcal{F}_{N,k}(\rho) \cdot e^{i[(Nm_0+k)\theta_t - Nn_0\varphi_t]} \tag{36}$$

where

$$\mathcal{F}_{N,k}(\rho) = \begin{cases} \rho^{|Nm_0+k|} & \text{for } 0 \le \rho \le 1, \\ \rho^{-|Nm_0+k|} & \text{for } \rho \ge 1. \end{cases} \tag{37}$$

Applying the boundary condition (26) it turns out that the lowest order term is given by

$$\Phi_M^{(0)i,\,e}(r_t,\ \theta_t,\ \varphi_t) = \mp\frac{\mu_0 I_h}{i\pi}\sum_{N=1}^{\infty}\sum_{k=-\infty}^{\infty}\frac{J_k(Nm_0\lambda)}{N}\left(\frac{r_t}{b_t}\right)^{\pm|Nm_0+k|} \cdot e^{i[(Nm_0+k)\theta_t - Nn_0\varphi_t]} \tag{38}$$

for both internal (upper signal) and external (lower signal) regions, and $J_k(x)$ is the Bessel function of $k$th order. Since the expansion coefficients fall down rapidly to zero as $N$ increases, only the $N = 1$ term is relevant in (38). By a similar reason, we conclude that if suffices to consider only those terms for which $|k| \le m_0$ in the second summation. With such simplifications, the scalar potential produced by an RHW is

$$\Phi_M^{(0)i,\,e}(r_t,\ \theta_t,\ \varphi_t) = \mp\frac{\mu_0 I_h}{i\pi}\sum_{k=-m_0}^{+m_0} J_k(m_0\lambda)\left(\frac{r_t}{b_t}\right)^{\pm(m_0+k)} \cdot e^{i[(m_0+k)\theta_t - n_0\varphi_t]} \tag{39}$$

The second coupled equation (35) is nonhomogeneous, so that its solution may be written as

$$\Phi_M^{(1)} = \Phi_M^{(p)} + \Phi_M^{(h)} \tag{40}$$

where a particular solution is

$$\Phi_M^{(p)i,\,e} = \frac{\mu_0 I_h}{i\pi} \sum_{k=-m_0}^{m_0} \left( c_k^{(p)i,\,e} \rho^{\pm(m_0+k)+1} e^{i(k\mp 1)\theta_t} \right) \cdot e^{-im_0\lambda \sin\theta_t} e^{iu_t} \tag{41}$$

whose coefficients are

$$c_k^{(p)i,\,e} = -J_k(m_0\lambda)\,\frac{2(m_0+k)\pm 1}{4}. \tag{42}$$

On the other hand, the general solution of the corresponding homogeneous equation is

$$\Phi_M^{(h)} = \sum_{k=-m_0}^{m_0} \left( c_k^{(+)} \mathcal{F}_k^{(+)}(\rho) e^{i(k+1)\theta_t} + c_k^{(-)} \mathcal{F}_k^{(-)}(\rho) e^{i(k-1)\theta_t} \right) \cdot e^{-im_0\lambda \sin\theta_t} e^{iu_t} \tag{43}$$

where

$$\mathcal{F}_k^{(\pm)}(\rho) = \begin{cases} \rho^{|m_0+k\pm 1|}, & \text{for } 0 \le \rho \le 1 \\ \rho^{-|m_0+k\pm 1|}, & \text{for } \rho \ge 1. \end{cases} \tag{44}$$

The coefficients $c_k^{(\pm)}$ are obtained by using (26) again, and solving a system of algebraic equation, resulting in

$$c_k^{(+)i,\,e} = -\frac{\mu_0 I_h}{2\pi i} \left\{ \left[ \frac{(m_0+k-1)}{|m_0+k+1|} \mp 1 \right] c_k^{(p)e} - \frac{(m_0+k)}{|m_0+k+1|}\, J_k(m_0\lambda) \right\} \tag{45}$$

$$c_k^{(-)i,\,e} = -\frac{\mu_0 I_h}{2\pi i} \left\{ \left[ \frac{(m_0+k+1)}{|m_0+k-1|} \pm 1 \right] c_k^{(p)i} + \frac{(m_0+k)}{|m_0+k-1|}\, J_k(m_0\lambda) \right\}. \tag{46}$$

Combining the zeroth- and first-order solutions in (29), we may write the contravariant components of the magnetic field generated by an RHW

$$B_h^1 = \frac{\partial \Phi_M^{(0)}}{\partial r_t} + \left( \frac{b_t}{R_0'} \right) \left[ \frac{\partial}{\partial r_t} \left( \Phi_M^{(p)} + \Phi_M^{(h)} \right) - 2\,\frac{r_t}{b_t}\,\frac{\partial \Phi_M^{(0)}}{\partial r_t} \cos\theta_t + \frac{1}{b_t}\,\frac{\partial \Phi_M^{(0)}}{\partial \theta_t} \sin\theta_t \right] \tag{47}$$

$$B_h^2 = \frac{1}{r_t^2}\,\frac{\partial \Phi_M^{(0)}}{\partial \theta_t} + \left( \frac{b_t}{R_0'} \right) \left[ \frac{1}{r_t^2}\,\frac{\partial}{\partial \theta_t} \left( \Phi_M^{(p)} + \Phi_M^{(h)} \right) + \frac{1}{b_t}\,\frac{\partial \Phi_M^{(0)}}{\partial r_t} \sin\theta_t \right] \tag{48}$$

$$B_h^3 = 0 \tag{49}$$

in which we retained first order powers of the inverse aspect ratio $b_t/R_0'$. Notice, however, that the zeroth order term already contains toroidal effects, since $r_t$ depends on both $r$ and $\theta$ [see (89)]. It is useful to compare this result with that obtained in the limit of cylindrical geometry. In this case, we neglect the Shafranov shift such that the magnetic axis coincides with the geometric minor axis ($R_0' \to R_0$); and the RHW has now a uniform pitch ($\lambda = 0$), so that the helical variable is simply $u_t \to m_0\theta - n_0\varphi$. In this limit, (47)–(49) reduce to those obtained in early works [38].

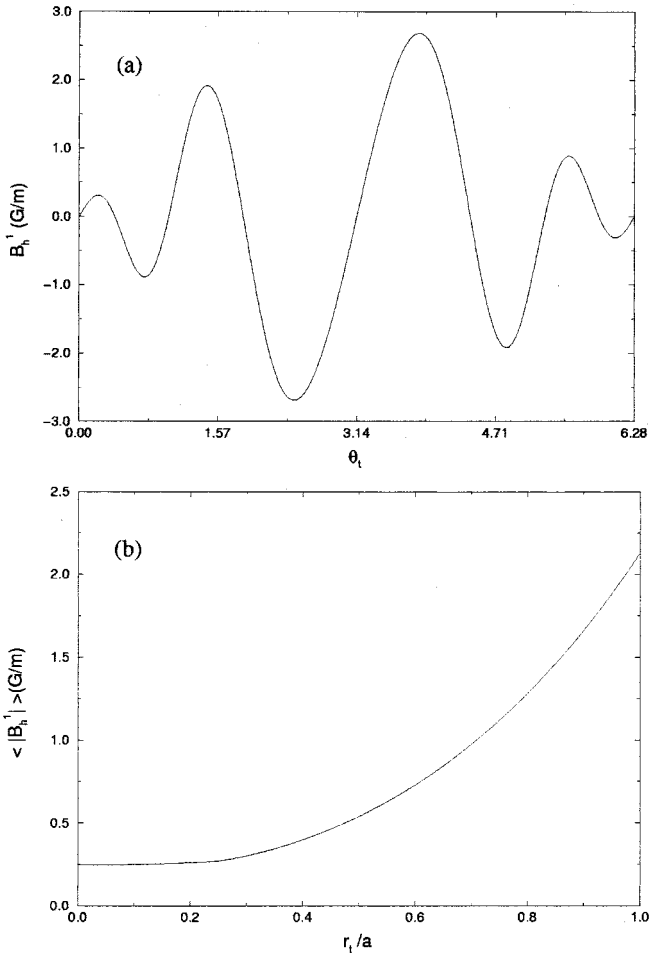


Fig. 4. Radial component of an RHW with $I_h/I_p = 0.003$, $(m_0,\, n_0) = (4,\, 1)$, and $\lambda = 0.4826$. (a) Poloidal profile, with $r_t/a = 0.91$; (b) radial profile, with $\theta_t = 5\pi/4$.

In Fig. 4(a), we show a poloidal profile of the radial component of the field generated by an RHW with $(m_0,\, n_0) = (4,\, 1)$, $(I_h/I_p) = 0.003$, $\lambda = 0.4826$, and at a fixed radial position $r_t/a = 0.911$. Other parameters are the same as those used in Fig. 1. We note that the poloidal perturbing field in the internal region (low $\theta_t$) is smaller than in the external region due to the effect of the toroidal curvature on the pitch of the RHW. Fig. 4(b) shows a radial profile of the poloidally averaged radial component, for similar parameters. It falls down rapidly when the radius decreases, so that only the plasma edge region is expected to be noticeably affected by the perturbing helical field.

## IV. Field Line Mapping for a Tokamak with Resonant Helical Windings

A field line mapping is obtained by following the paths of a given number of magnetic field lines and registering their intersections with a specified ($\varphi$ = const.) surface of section. Hence, it is a "time"-$2\pi$ stroboscopic sampling of the flow. The

solenoidal character of the magnetic field implies that the magnetic flux through any closed curve on this plane must be conserved, so that the field line mapping must be symplectic, or area-preserving. In some cases, it turns to be possible to derive an analytical form of the map equations, as we will see in the next section for a CML. However, more often we have to solve numerically the magnetic field line equations $(\mathbf{B}_0 + \mathbf{B}_h) \times \mathbf{d}\ell = \mathbf{0}$, which is a very time-consuming computational task, and poses a difficulty when one is investigating the long term behavior of field lines, for studies of diffusivity and loss due to collisions with the tokamak wall.

In this section, we will obtain such a map for the case of a tokamak with RHW, using the model fields of the two preceding sections. Initially, however, we will show how to compute the parameter $\lambda$ that appear in the winding law (24) of an RHW. Using (20) and (22), the field line equations in the unperturbed (equilibrium) configuration are

$$\frac{dr_t}{d\varphi_t} = 0 \tag{50}$$

$$\frac{d\theta_t}{d\varphi_t} = \frac{1}{q_c(r_t)}\left[1 - 2\,\frac{r_t}{R_0'}\,\cos\,\theta_t\right]. \tag{51}$$

Denoting the initial conditions as $(r_t^{(0)},\, \theta_t^{(0)},\, \varphi_t^{(0)} = 0)$, these equations may be integrated to give, for arbitrary $0 \le \varphi_t < 2\pi$, the following relations:

$$r_t(\varphi_t) = r_t^{(0)} \tag{52}$$

$$\theta_t(\varphi_t) = 2\,\arctan\left[\frac{\Omega\left(r_t^{(0)}\right)\sin\left(\dfrac{1}{q(r_t^{(0)})}\,\varphi_t + \Gamma\left(r_t^{(0)},\, \theta_t^{(0)}\right)\right)}{1 + \cos\left(\dfrac{1}{q(r_t^{(0)})}\,\varphi_t + \Gamma\left(r_t^{(0)},\, \theta_t^{(0)}\right)\right)}\right] \tag{53}$$

where

$$\Omega(r_t) = \left(1 - 2\,\frac{r_t}{R_0'}\right)^{1/2}\left(1 + 2\,\frac{r_t}{R_0'}\right)^{-1/2} \tag{54}$$

$$\Gamma(r_t,\, \theta_t) = 2\,\arctan\left[\frac{1}{\Omega(r_t)}\left(\frac{\sin\,\theta_t}{1 + \cos\,\theta_t}\right)\right]. \tag{55}$$

This exact solution of the unperturbed case enables us to compare the actual path of a field line at equilibrium with the path followed by a constant pitch helix, in which $m_0\theta_t - n_0\varphi_t =$ constant (Fig. 5). The difference between these paths is due to the toroidal geometry effect. Since one is interested in the resonant effects, the design of an RHW should reflect the actual path of the field lines, so we have to include this effect in the corresponding winding law. This is accomplished by defining another poloidal angle, as done by Boozer [32]

$$\begin{aligned}\vartheta(r_t,\, \theta_t) &= \frac{1}{q(r_t)}\int_0^{\theta_t}\frac{B_0^3(r_t,\, \theta_t)}{B_0^2(r_t,\, \theta_t)}\,d\theta \\ &= \left(1 - 4\left(\frac{r_t}{R_0'}\right)^2\right)^{1/2}\int_0^{\theta_t}\frac{d\theta}{1 - 2\,\dfrac{r_t}{R_0'}\,\cos\,\theta} \\ &= 2\,\arctan\left[\frac{1}{\Omega(r_t)}\left(\frac{\sin\,\theta_t}{1 + \cos\,\theta_t}\right)\right]\end{aligned} \tag{56}$$

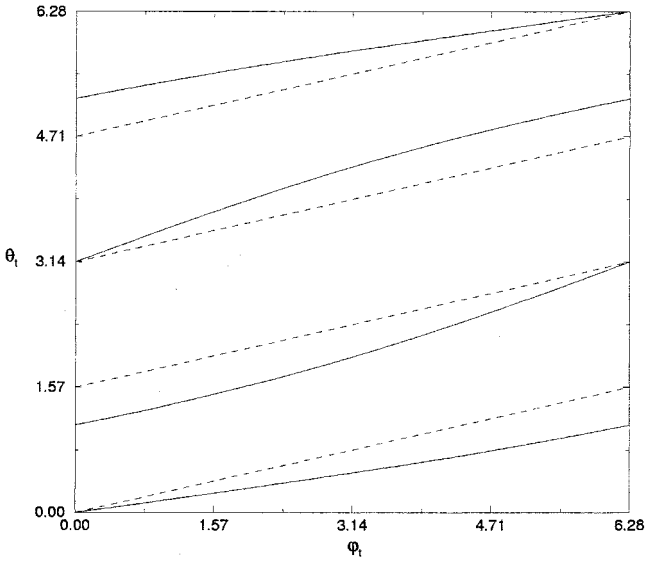


Fig. 5. Equilibrium magnetic field line path on a rational magnetic surface with $q = 4 : 1$. The straight dashed lines correspond to a helix of constant pitch.

which makes it possible to rewrite the winding law in the form $m_0\vartheta(r_t,\, \theta_t) - n_0\varphi_t =$ constant. Expanding (56) in Fourier series, and retaining only the lowest-order nonvanishing correction, we have for this new poloidal angle

$$\vartheta(\theta_t) = \theta_t + \lambda\,\sin\,\theta_t \tag{57}$$

where

$$\lambda = \left(1 - 4\left(\frac{r_t}{R_0'}\right)^2\right)^{1/2}\sum_{k=0}^{\infty}\frac{2(2k+1)!}{k!(k+1)!}\left(\frac{r_t}{R_0'}\right)^{2k+1} \tag{58}$$

which gives the winding law (24) with the appropriate value of $\lambda$. In our case, since we are interested in obtaining a resonant effect on the rational magnetic surface with $q = 4 : 1$, we need an RHW with $(m_0,\, n_0) = (4,\, 1)$. This leads to $\lambda = 0.4827$, as it was already used in Fig. 4.

We will consider the action of an RHW as a superposition of the equilibrium (6)–(8) and perturbing fields (47)–(49), neglecting the plasma response. This approximation works well, provided we are far from marginal equilibrium states. The field line equations in the presence of perturbation are now written in the form

$$\frac{dr_t}{d\varphi_t} = \frac{B_h^1(r_t, \theta_t,\, \varphi_t)}{B_0^3(r_t,\, \theta_t,\, \varphi_t)} \tag{59}$$

$$\frac{d\theta_t}{d\varphi_t} = \frac{B_0^2(r_t,\, \theta_t,\, \varphi_t) + B_h^2(r_t,\, \theta_t,\, \varphi_t)}{B_0^3(r_t,\, \theta_t,\, \varphi_t)}. \tag{60}$$

Unlike the unperturbed case, we can not find an analytical solution for this set of differential equations, and we have to use numerical integration (Bulirsch–Stoer method with Richardson extrapolation [39]). We begin with a single initial condition $(r_t^{(0)},\, \theta_t^{(0)},\, \varphi_t^{(0)} = 0)$. Any time a field line passes through the $\varphi = 0$ plane, we record the coordinates $(r_t,\, \theta_t)$ of the point and repeat this process a large number of times, which generates an orbit, or trajectory, in the dynamical systems language. Next, we choose another initial condition, generate a new orbit, and so on.

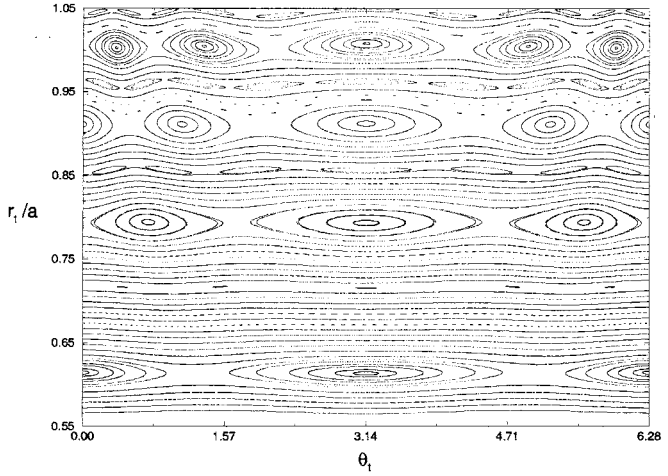


(a)

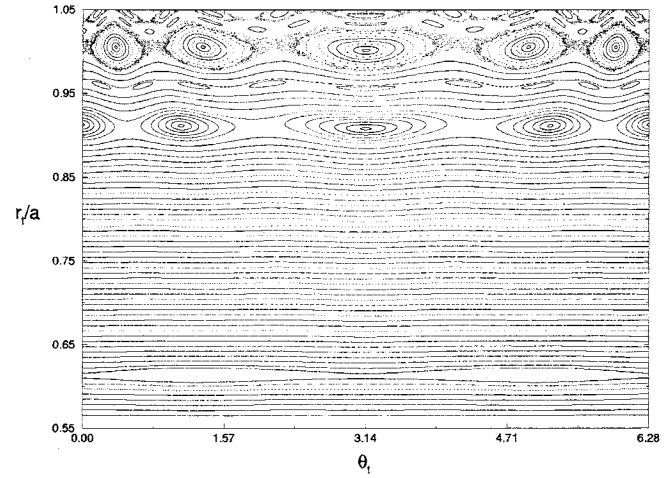


(b)

Fig. 6. Phase portrait, in polar toroidal coordinates, of field lines for an RHW with $(m_0,\ n_0) = (4,\ 1)$, $I_h/I_p = 0.001$, and: (a) $\lambda = 0.4827$; (b) $\lambda = 0$.

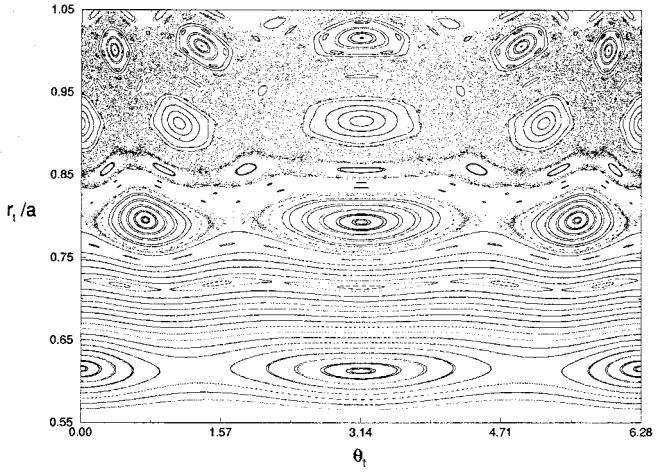


(a)

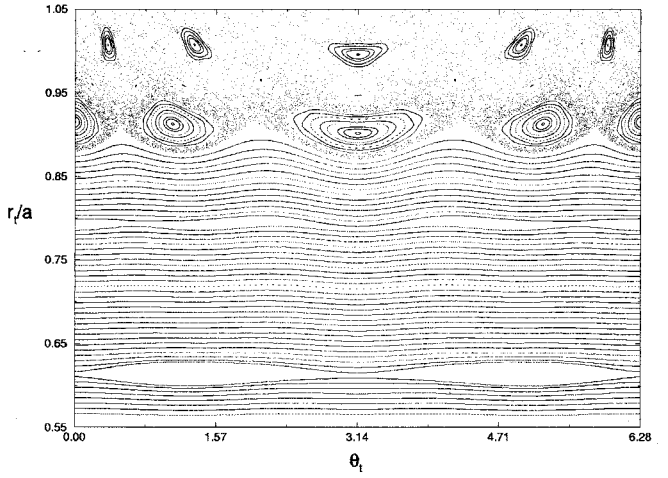


(b)

Fig. 7. Phase portrait, in polar toroidal coordinates, of field lines for an RHW with $(m_0,\ n_0) = (4,\ 1)$, $I_h/I_p = 0.003$, and: (a) $\lambda = 0.4827$; (b) $\lambda = 0$.

In Fig. 6(a), we present a phase portrait of a $(m_0, n_0) = (4, 1)$ RHW in which the current is 0.1% of the total plasma current, and $\lambda = 0.4827$, as given by (58). The Poincaré section at $\varphi = 0$ was deformed to a rectangular shape for the sake of clarity. We can identify many magnetic island chains over the depicted portion of the plasma column (in fact, Hamiltonian dynamics ensures that there is an infinite number of these chains, centered at all rational magnetic surfaces [22]). The main island to be excited by the RHW is centered at a former magnetic surface with safety factor equal to $q = 4:1$, consistently with the mode numbers here chosen. Other noticeable islands have safety factors $5:1$, $3:1$ and $2:1$, for example. In order to see the effect of the $\lambda$ parameter on the field line structure, we show in Fig. 6(b) the same phase portrait, but with $\lambda = 0$. It is apparent that the number of sizeable island chains has been reduced in this case. In particular, the $2:1$ and $3:1$ islands have their widths dramatically decreased. Hence, the use of a winding law such as (24) enhances the resonant effect produced by an RHW.

The RHW current in Fig. 7(a) has been increased to 0.3% of the plasma current and Fig. 7(b) is the corresponding case with vanishing $\lambda$. We still see many island chains besides the main $4:1$ one, but there are some differences. First, the islands' widths have increased. In fact, by application of a Hamiltonian perturbation theory, one finds that these widths increase as $(I_h)^{1/2}$ [30]. Secondly, in the region near to the island separatrix, there are thin area-filling portions where the field lines are chaotic. Both facts are explained by standard results of Hamiltonian dynamics, like the KAM and Poincaré–Birkhoff theorems.

The fate of a magnetic surface, after the application of a small perturbation, is basically determined by its safety factor $q$, which is the inverse of the winding number of the trajectories lying on the surface [4]. If $q$ is an irrational number, and if the perturbation is weak enough, the celebrated KAM theorem states that most of these surfaces will survive, even though with some deformation [22]. This is clearly seen in the remaining surfaces that separate neighbor island chains, as in Fig. 6(a). Now, if $q$ is a rational number, as the $4:1$ chain just mentioned, the Poincaré–Birkhoff theorem says that the corresponding surface will disappear, leaving an even number of fixed points, half of them stable and half unstable. The stable (or elliptic) points are the centers of the islands, whereas the unstable (or

hyperbolic) points are at the crossings of their separatrices. However, after the application of a nonsymmetric perturbation, it may be proven that these separatrices will intercept each other an infinite number of times (homoclinic crossings) forming a region of chaotic dynamics there, in the sense that the corresponding Lyapunov exponent is positive [40].

In Fig. 6(b), we may already see such a region of limited chaotic motion in the neighborhood of the separatrices of the 4 : 1 island chain. The other chains have their own chaotic regions, but they are not so evident, either due to their small widths or the initial conditions used in the phase portrait failed to generate an orbit in the chaotic region. As long as the perturbation is small enough, however, these locally chaotic regions are separated from each other by surviving magnetic surfaces, and the radial excursion of field lines is naturally limited by them. On the other hand, as the perturbation strength increases, the islands' widths also increase, and the surviving surfaces are progressively engulfed by locally chaotic regions belonging to adjacent island chains, as illustrated in Fig. 7(a) and (b). The adjacent island chains over a given region may be so large that the entire region around them is filled with chaotic field lines. This eventually leads to a globally chaotic region where large-scale chaotic excursions are possible. In the limit of very large perturbation strength, even the elliptic points in the islands' centers may lose their stability and bifurcate, generating other periodic orbits.

## V. Field Line Mapping due to a Chaotic Magnetic Limiter

The nonsymmetric character of the magnetic field generated by an RHW is due to the toroidal effect on the former helical symmetry. This breaks the integrability (in the Hamiltonian sense) of the equilibrium configuration, thus leading to all the consequences mentioned in the last section, the most important to us being the generation of chaotic field lines. Remember that, from the point of view of reducing plasma-wall interactions, it would be useful to create such a chaotic region in the peripheral region of the plasma column. In principle, this is feasible by using an RHW with appropriate values of $(m_0, n_0)$, as the 4 : 1 case here studied. However, the mounting of such windings on a tokamaks is sometimes difficult, because of the large number of windows for diagnostic purposes along the tokamak wall. This has led to the concept of a CML [27].

The CML design consists of one or more slices of an RHW with adequate mode numbers, located in suitable positions along the torus. Hence, a CML is quite different from an RHW, in the sense that in the former the perturbing field will break the axisymmetry due to an explicit $\varphi$-dependence. On the other hand, for some ergodic divertors the $\theta$-symmetry is broken by coils wound around the torus over a limited poloidal range $\pi + \theta_c \leq \theta \leq \pi - \theta_c$ [5]. In the following, we will consider a CML with $N_a$ current rings located symmetrically along the toroidal circumference of the tokamak, each of them being a slice of length $\ell$ of an RHW with mode numbers $(m_0, n_0)$, and a winding law given by (24) (Fig. 8). Ignoring, at first, the finite extension of the CML rings, the magnetic field $\mathbf{B}_L$ produced by such a configuration was already derived in Section III. Here, it is convenient to express it using the vector potential: $\mathbf{B}_L = \nabla \times \mathbf{A}_L$.

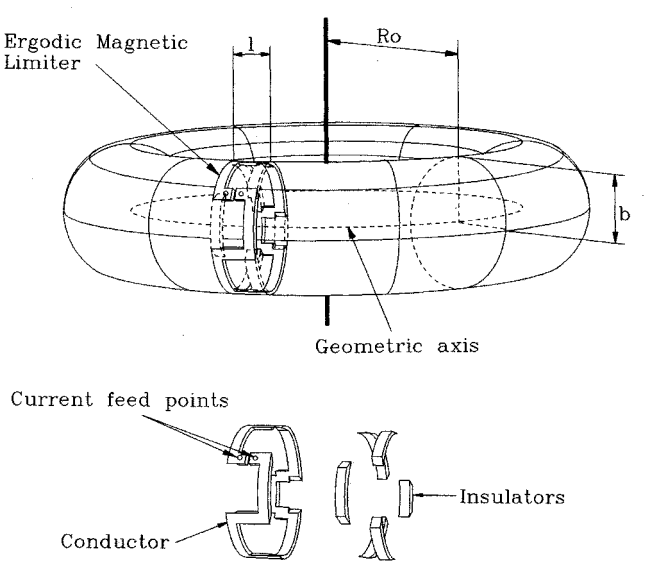


Fig. 8. Scheme of a chaotic magnetic limiter in a tokamak. In detail, we show the design of a single ring.

Here, only the lowest order solution is necessary, since for a CML with small length $\ell$, one may neglect all toroidal effects on the field it generates. From (41) and (43), we have that the vector potential component of interest is

$$A_{L3}(r_t, \theta_t, \varphi_t) = -\frac{\mu_0 I_h R_0'}{\pi} \sum_{k=-m_0}^{+m_0} J_k(m_o\lambda) \left(\frac{r_t}{b_t}\right)^{m_0+k} \cdot e^{i[(m_0+k)\theta_t - n_0\varphi_t]} \tag{61}$$

from which the CML contravariant field components are given by

$$B_L^1 = -\frac{1}{R_0' r_t} \frac{\partial A_{L3}}{\partial \theta_t} \tag{62}$$

$$B_L^2 = \frac{1}{R_0' r_t} \frac{\partial A_{L3}}{\partial r_t} \tag{63}$$

and the model field will be the superposition between the equilibrium and limiter fields: $\mathbf{B} = \mathbf{B}_0 + \mathbf{B}_L$.

The magnetic field line equations (20) are, thus

$$\frac{dr_t}{d\varphi_t} = -\frac{1}{r_t B_T}\left(1 - 2\frac{r_t}{R_0'}\cos\theta_t\right)\frac{\partial}{\partial \theta_t} \cdot [\Psi_{p0}(r_t) + A_{L3}(r_t, \theta_t, \varphi_t)] \tag{64}$$

$$\frac{d\theta_t}{d\varphi_t} = \frac{1}{r_t B_T}\left(1 - 2\frac{r_t}{R_0'}\cos\theta_t\right)\frac{\partial}{\partial r_t} \cdot [\Psi_{p0}(r_t) + A_{L3}(r_t, \theta_t, \varphi_t)] \tag{65}$$

where $B_T \equiv \mu_0 I_e / 2\pi R_0'$ is the toroidal magnetic field on the magnetic axis.

In order to use a Hamiltonian formulation for the field line flow, we shall define canonical action and angle variables. The canonical angle will be the $\vartheta$-variable defined in (56), whereas

its conjugate action will be defined in terms of the normalized toroidal magnetic flux

$$\mathcal{J}(r_t) = \frac{1}{2\pi {R'_0}^2 B_T} \int \mathbf{B}_0.\mathbf{d}\sigma_3 = \frac{1}{4}\left[1 - \left(1 - 4\frac{r_t^2}{{R'_0}^2}\right)^{1/2}\right] \tag{66}$$

where $\mathbf{d}\sigma_3 = R'_0 r_t\, dr_t\, d\theta_t \hat{e}^3$. Note that $\mathcal{J}(r_t) \geq 0$ for any $r_t \geq 0$. Expanding this action in powers of the aspect ratio gives, for the lowest order, the variable $r_t^2/2$ used in related works [30]. The time-like variable will be the ignorable coordinate $t = \varphi_t$.

The field line equations (59) and (60) may be cast in a canonical form [3]

$$\frac{d\mathcal{J}}{dt} = -\frac{\partial H}{\partial \vartheta} \tag{67}$$

$$\frac{d\vartheta}{dt} = \frac{\partial H}{\partial \mathcal{J}} \tag{68}$$

with the Hamiltonian

$$\begin{aligned} H(\mathcal{J}, \vartheta, t) &= H_0(\mathcal{J}) + H_1(\mathcal{J}, \vartheta, t) \\ &= \frac{1}{B_T {R'_0}^2}\, \Psi_{p0}(\mathcal{J}) + \frac{1}{B_T {R'_0}^2}\, A_{L3}(\mathcal{J}, \vartheta, t). \end{aligned} \tag{69}$$

However, it turns out that the length of each limiter ring $\ell$ is just a small fraction of the toroidal circumference $2\pi R'_0$. If $\ell$ is small enough, we can model the CML effect as a sequence of delta-functions centered at each ring position [29]. So, we suppose the following Hamiltonian of the tokamak with a CML

$$H_L(\mathcal{J}, \vartheta, t) = H_0(\mathcal{J}) + \frac{\ell}{R'_0} H_1(\mathcal{J}, \vartheta, t) \sum_{k=-\infty}^{+\infty} \delta\left(t - k\frac{2\pi}{N_a}\right) \tag{70}$$

where $H_0$ and $H_1$ are the same as in (69).

Unlike the RHW case previously studied, the impulsive character of the perturbation enables us to analytically obtain a field line map. In this work, we will ensure the symplectic nature of the map by using explicit canonical action-angle variables. Accordingly, we define $\mathcal{J}_n$ and $\vartheta_n$ as the action and angle variables, respectively, at the $n$th crossing of a field line with the plane $\varphi_k = t_k = 2\pi k/N_a$, with $k = 0, 1, 2, \ldots, N_a - 1$ [41]. Viana and Caldas have used local coordinates to derive such a map [42], which was later improved by Ullmann and Caldas by the use of a generating function [43], since the map $(\mathcal{J}_n, \vartheta_n) \rightarrow (\mathcal{J}_{n+1}, \vartheta_{n+1})$ may be regarded as a canonical transformation.

Integrating the Hamilton equations (67) and (68) for the CML, Hamiltonian (70) gives the following area-preserving mapping for the near-integrable system

$$\mathcal{J}_{n+1} = \mathcal{J}_n - \epsilon\left(\frac{\partial H_1}{\partial \vartheta}\right)(\mathcal{J}_{n+1}, \vartheta_n, t_n) \tag{71}$$

$$\vartheta_{n+1} = \vartheta_n + \frac{2\pi}{N_a q(\mathcal{J}_{n+1})} + \epsilon\left(\frac{\partial H_1}{\partial \mathcal{J}}\right)(\mathcal{J}_{n+1}, \vartheta_n, t_n) \tag{72}$$

$$t_{n+1} = t_n + \frac{2\pi}{N_a} \tag{73}$$

where the dimensionless perturbation parameter is

$$\epsilon = -2\left(\frac{\ell}{2\pi R'_0}\right)\frac{I_h}{I}. \tag{74}$$

One should note, however, that there is no rigorous derivation of the map (71)–(73) from the Hamiltonian function (70) because the integration along the delta functions is not well defined. A general perturbative procedure of construction of symplectic maps for Hamiltonian systems of the type (70) has been recently developed [44], [12].

Combining the perturbing field (61) with the limiter Hamiltonian (70) results as

$$H_1(\mathcal{J}, \vartheta, t) = \sum_{m'=0}^{2m_0} H_{m'}(r_t(\mathcal{J}))e^{i[m'\theta_t(\mathcal{J}, \vartheta) - n_0 t]} \tag{75}$$

with coefficients given by

$$H_{m'}(r_t) = -J_{m'-m_0}(m_0\lambda)\left(\frac{r_t}{b_t}\right)^{m'} \tag{76}$$

and $r_t(\mathcal{J})$ is obtained by inverting (66). It is useful to expand in a Fourier series the perturbing Hamiltonian in action-angle variables

$$H_1(\mathcal{J}, \vartheta, t) = \sum_{n=0}^{2m_0} H_n^*(\mathcal{J})e^{i(n\vartheta - n_0 t)} \tag{77}$$

where the corresponding coefficients are

$$H_m^*(\mathcal{J}) = \sum_{m'=0}^{2m_0} H_{m'}(r_t(\mathcal{J}))S_{m,m'}(\mathcal{J}) \tag{78}$$

in which we defined

$$\begin{aligned} S_{m,m'}(\mathcal{J}) = (-1)^m \left(\frac{c_1(\mathcal{J})}{c_2(\mathcal{J})}\right)^{m+m'} \sum_{n=0}^{m} (-1)^n \alpha_n \\ \cdot (m, m')\left(\frac{c_1(\mathcal{J})}{c_2(\mathcal{J})}\right)^{-2n} \end{aligned} \tag{79}$$

with

$$c_1(\mathcal{J}) = 1 - \frac{1}{\Omega(r_t(\mathcal{J}))} \tag{80}$$

$$c_2(\mathcal{J}) = 1 + \frac{1}{\Omega(r_t(\mathcal{J}))} \tag{81}$$

$$\alpha_n(m, m') = \begin{cases} 1, & \text{if } m = 0 \text{ and } n = 0 \\ m', & \text{if } m = 1 \text{ and } n = 0 \text{ or } n = 1 \\ m'\dfrac{(m+m'-n-1)!}{(m-n)!(m'-n)!n!}, & \text{if } m > 1 \text{ and } n \leq m' \\ 0, & \text{if } m > 1 \text{ and } n > m' \end{cases} \tag{82}$$

and $\Omega(r_t)$ is given by (54).

Fig. 9(a) shows a phase portrait of the map (71)–(73) for a CML with $N_a = 4$ current rings, each of them with being a slice of an RHW with $(m_0, n_0) = (4, 1)$ and $\lambda = 0.4827$, carrying

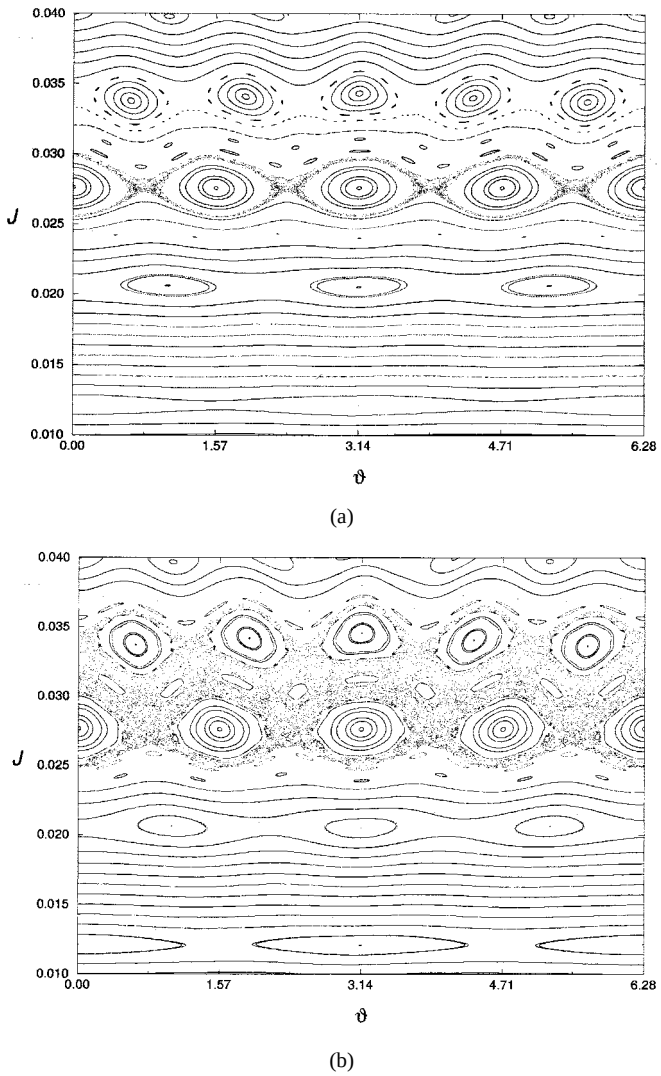


Fig. 9. Phase portrait, in canonical coordinates, of field lines for a CML with $N_a = 4$ rings, $(m_0, n_0) = (4, 1)$, $\lambda = 0.4827$, and: (a) $I_h/I_p = 0.0010$; (b) $I_h/I_p = 0.0015$.

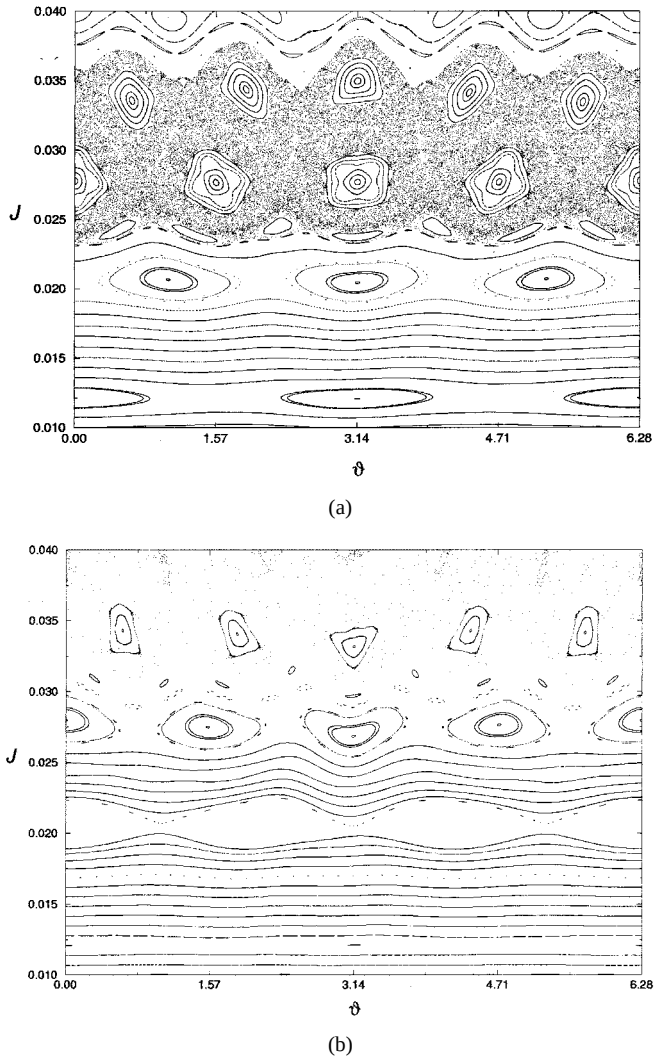


Fig. 10. Phase portrait, in canonical coordinates, of field lines for a CML with $N_a = 4$ rings, $(m_0, n_0) = (4, 1)$, $I_h/I_p = 0.0025$, and: (a) $\lambda = 0.4827$; (b) $\lambda = 0$.

a current of 1.0% of the plasma current $I_p$. The tokamak equilibrium parameters are the same as in the case of RHW, as considered in the previous sections. We see again a main $q = 4 : 1$ island chain at $\mathcal{J} \approx 0.027$, which corresponds to a normalized radius $r_t/a \approx 0.9$. This means that this island chain, and the corresponding local chaotic region around its separatrix, is located near the plasma edge. These main islands are surrounded by satellite chains with $q = 3 : 1$ and $q = 5 : 1$, which appear due to the toroidicity effect.

The CML current has been raised to 1.5% of the plasma current in Fig. 9(b), showing that, for this higher limiter current, the 4 : 1 and 5 : 1 chains have already partially overlapped, fusing their chaotic regions into a large-scale chaotic layer that extends over a larger peripheral portion of the plasma column. In both cases, the chaotic region, although comprising the plasma edge region, does not reach the tokamak wall, due to the existence of many surviving magnetic surfaces in between. If we increase further the limiter current, the chaotic region will become even more pronounced, as we illustrate in Fig. 10(a) for $I_h$ equal to 2.5% of $I_p$, but it still does not reach the wall.

It turns out that there is another and cheaper way to make the chaotic region touch the inner wall, namely to set up $\lambda = 0$. In this case, with the same current as before, the chaotic region reaches the wall [Fig. 10(b)]. Hence, a nonzero $\lambda$ would require a higher limiter current for the operation of a CML. The positive feature of choosing an appropriate $\lambda \neq 0$ is to obtain a chaotic region that is concentrated around a main resonance (the 4 : 1 one, in our case), but for a wide peripheric chaotic region it would be preferable to use $\lambda = 0$.

## VI. Conclusion

Since chaotic dynamics in general implies both irregular behavior and loss of predictability for large times, it would be a bad feature of real systems and much effort could be necessary to avoid, or at least control it. However, chaotic dynamics, if properly used, may be a useful tool in plasma fusion machines. We have explored in this paper two aspects of this idea. In the situations investigated in this paper, chaotic magnetic field line behavior is generated by nonsymmetric magnetostatic perturbations applied on the tokamak equilibrium field. We have consid-

ered a tokamak equilibrium model magnetic field which is quite realistic in the sense that it uses the following:

1) proper geometry (polar toroidal coordinates);
2) self-consistent treatment for the equilibrium magnetic field (it is obtained by solving an equilibrium MHD equation);
3) plasma current profile that is compatible with results of tokamak experiments.

The first type of nonsymmetric perturbation we study is due to RHW, whose main goal is to create a region of chaotic field lines in the plasma column, with the purpose of studying minor disruptive instabilities. The magnetic field generated by RHW was analytically obtained through solving Laplace equation in polar toroidal coordinates. A distinctive characteristic of our model is the presence of a winding law for RHW, which reproduces the actual paths of equilibrium field lines and gives an enhanced resonant effect. Our results were shown in the form of a field line map obtained by numerical integration of the corresponding equations. Furthermore, it is possible to obtain, in terms of action-angle variables, a Hamiltonian formalism by considering lowest order terms only.

The second perturbation type is due to a CML, which consists of external current rings, designed so as to create a chaotic field line region in the peripheral region of the plasma column, with the purpose of controlling plasma-wall interactions. The field line Hamiltonian for this system was obtained by supposing a sequence of delta-function pulses, and the map was analytically determined. It satisfies the necessary conditions described by Balescu [4] for a consistent description of field line behavior: 1) it is a symplectic map in the sense that the Hamiltonian structure of the field line equations is reflected in the map, since it is written in terms of action-angle variables; and 2) it is compatible with toroidal geometry, since our action variable $\mathcal{J}$ is always a nonnegative number, i.e., a field line starting on the magnetic axis may either remain on the axis or move to a positive $\mathcal{J}$, but never to a negative $\mathcal{J}$. We remark that the second condition is not fulfilled by the Chirikov–Taylor standard map [40], for example.

A similar procedure was followed by Abdullaev *et al.* to obtain a symplectic map that describes the dynamics of an ergodic divertor in a toroidal system [12]. Our map for CML has proven to be useful to study problems that need long term integration of field line equations, like diffusion and bifurcation effects [45]. We have shown that an adequate choice of CML parameters may create this chaotic region in the plasma edge region. When a chaotic field line escapes from the plasma region and enters the vacuum region that surrounds the plasma, it will eventually collide with the wall, resulting in a loss of field lines. A detailed study of field line diffusion in the plasma edge, and the question of how field lines are lost due to collisions, is addressed in another paper to be published elsewhere [46].

## APPENDIX

Here, we describe the polar toroidal coordinate system used in this paper to describe both equilibrium and perturbing fields. A cylindrical system $(R, Z, \phi)$ may be used to describe the tokamak, in which the symmetry $(Z)$ axis is the major axis of the torus, $R$ is the radial distance from this axis, and $\phi$ is the azimuthal angle (see Fig. 1). The local coordinates $(r, \theta, \varphi)$ are related to these variables by the following:

$$\begin{aligned} R &= R_0 - r\cos\theta \\ Z &= r\sin\theta \\ \phi &= \varphi. \end{aligned} \tag{83}$$

The toroidal coordinates $(\xi, \omega, \varphi)$ are defined as [47]

$$\begin{aligned} R &= \frac{R_0' \sinh\xi}{\cosh\xi - \cos\omega} \\ Z &= \frac{R_0' \sin\omega}{\cosh\xi - \cos\omega} \\ \phi &= \varphi \end{aligned} \tag{84}$$

in such a way that the coordinate surfaces on which $\xi = \text{const}$ are tori with minor radii $a = R_0'/\sinh\xi$, and major radii $R_0'\coth\xi$.

The polar toroidal coordinates $(r_t, \theta_t, \varphi_t)$ may be defined in terms of the toroidal coordinates by the following [34]:

$$\begin{aligned} r_t &= \frac{R_0'}{\cosh\xi - \cos\omega} \\ \theta_t &= \pi - \omega \\ \varphi_t &= \varphi. \end{aligned} \tag{85}$$

The $r_t = \text{const.}$ curves have a pronounced curvature in the interior region of the torus, from where we start counting poloidal $(\theta_t)$ angles. In Fig. 11, we depict some coordinate surfaces of this system.

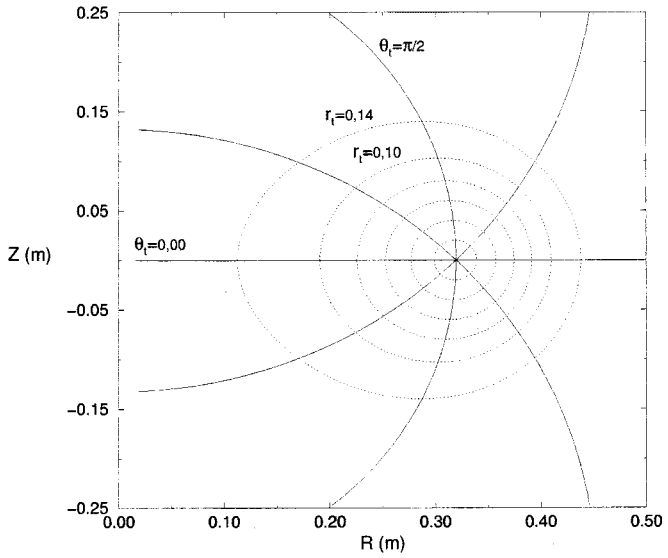


Fig. 11. Coordinate surfaces of the polar toroidal coordinate system, at a $\varphi = 0$ section.

The contravariant basis vectors are

$$\begin{aligned} \hat{e}^1 &= -\frac{r_t}{R_0'}\left(\sinh\xi\hat{e}_\xi + \sin\theta_t\hat{e}_\omega\right) \\ \hat{e}^2 &= -\frac{1}{r_t}\hat{e}_\omega \\ \hat{e}^3 &= -\frac{1}{r_t\sinh\xi}\hat{e}_\xi \end{aligned} \tag{86}$$

and the contravariant metric tensor elements are

$$g^{11} = 1 - 2\frac{r_t}{R_0'}\cos\theta_t, \quad g^{12} = g^{21} = \frac{1}{R_0'}\sin\theta_t$$
$$g^{13} = g^{31} = 0, \quad g^{22} = \frac{1}{r_t^2}, \quad g^{23} = g^{32} = 0, \quad g^{33} = \frac{1}{R^2}, \tag{87}$$

where

$$R^2 = R_0'^2\left[1 - 2\left(\frac{r_t}{R_0'}\right)\cos\theta_t - \left(\frac{r_t}{R_0'}\right)^2\sin^2\theta_t\right] \tag{88}$$

and $\sqrt{g} = R_0' r_t$. Since there are nonvanishing off-diagonal elements, this is a nonorthogonal system.

The relations between local and polar toroidal coordinates are

$$r_t = r\left[1 - \left(\frac{r}{R_0'}\right)\cos\theta - \left(\frac{r}{2R_0'}\right)^2\right]^{1/2} \tag{89}$$

$$\sin\theta_t = \sin\theta\left[1 - \left(\frac{r}{R_0'}\right)\cos\theta - \left(\frac{r}{2R_0'}\right)^2\right]^{-1/2} \tag{90}$$

showing that the polar toroidal coordinates tend to the local ones in the large aspect ratio limit ($r \ll R_0'$).

## ACKNOWLEDGMENT

I. L. Caldas wishes to thank S. McCool and W. A. Craven, University of Texas at Austin, for the useful discussions and valuable suggestions about CML design.

## REFERENCES

[1] J. Wesson, *Tokamaks*. Oxford, U.K.: Oxford Univ. Press, 1982.
[2] J. P. Friedberg, *Ideal Magnetohydrodynamics*. New York: Plenum, 1987.
[3] K. J. Whiteman, "Invariants and stability in classical mechanics," *Rep. Prog. Phys.*, vol. 40, pp. 1033–1069, 1977.
[4] R. Balescu, M. Vlad, and F. Spineanu, "Tokamap: A Hamiltonian twist map for magnetic field lines in a toroidal geometry," *Phys. Rev. E, Stat. Phys. Plasmas Fluids Relat. Interdiscip. Top.*, vol. 58, p. 951, July 1998.
[5] S. S. Abdullaev, K. H. Finken, A. Kaleck, and K. H. Spatschek, "Twist mapping for the dynamics of magnetic field lines in a tokamak ergodic divertor," *Phys. Plasmas*, vol. 5, p. 196, 1998.
[6] J. P. Morrison, "Magnetic field lines, Hamiltonian dynamics and nontwist systems," *Phys. Plasmas*, vol. 7, p. 2279, June 2000.
[7] S. C. McCool *et al.*, "Electron thermal confinement studies with applied resonant fields on TEXT," *Nucl. Fusion*, vol. 29, p. 547, 1989.
[8] P. Ghendrih, A. Grosman, and H. Capes, "Theoretical and experimental investigations of stochastic boundaries in tokamaks," *Plasma Phys. Control. Fusion*, vol. 38, pp. 1653–1724, Oct. 1996.
[9] K. H. Finken, Ed., "Special issue on dynamic ergodic divertor," in *Fusion Eng. Des.*, 1997, vol. 37, p. 335.
[10] A. Punjabi, A. Verma, and A. Boozer, "Stochastic broadening of the separatrix of a tokamak divertor," *Phys. Rev. Lett.*, vol. 69, p. 3322, Dec. 1992.
[11] A. Punjabi, H. Ali, and A. Boozer, "Symmetric simple map for a single-null divertor tokamak," *Phys. Plasmas*, vol. 4, p. 337, 1997.
[12] S. S. Abdullaev, K. H. Finken, and K. H. Spatschek, "Asymptotical and mapping methods in study of ergodic divertor magnetic field in a toroidal system," *Phys. Plasmas*, vol. 6, p. 153, Jan. 1999.
[13] H. Wobig, "Magnetic surfaces and localized perturbations in the Wendelstein VII–A Stellarator," *Z. Naturforsch.*, vol. 42a, pp. 1054–1066, Oct. 1987.
[14] F. Karger and F. Lackner, "Resonant helical divertor," *Phys. Lett. A*, vol. 61, pp. 385–387, June 1975.
[15] W. Engelhardt and W. Feneberg, "Influence of an ergodic magnetic limiter on the impurity content in a tokamak," *J. Nucl. Mater.*, vol. 76/77, p. 518, 1978.
[16] D. C. Robinson, "Ten years of results from the TOSCA device," *Nucl. Fusion*, vol. 25, pp. 1101–1108, 1985.
[17] Pulsator Team, "The Pulsator tokamak," *Nucl. Fusion*, vol. 25, p. 1059, 1985.
[18] A. J. Wootton, B. A. Carreras, H. Matsumoto, K. McGuire, W. A. Peebles, C. P. Ritz, P. W. Terry, and S. J. Sweben, "Fluctuations and anomalous transport in tokamaks," *Phys. Fluids*, vol. 2, p. 2879, 1990.
[19] I. H. Tan, I. L. Caldas, I. C. Nascimento, R. P. Silva, E. K. Sanada, and R. Bruha, "Mirnov oscillations in a small tokamak," *IEEE Trans. Plasma Sci.*, vol. PS-14, pp. 279–281, Mar. 1986.
[20] K. M. McGuire and D. C. Robinson, "Magnetic islands and disruptions in a tokamak," in *Proc. 9th Eur. Conf. on Controlled Fusion and Plasma Physics*, vol. 1, 1979, p. 93.
[21] A. Vannucci, I. C. Nascimento, and I. L. Caldas, "Disruptive instabilities in the discharge of the TBR-1 tokamak," *Plasma Phys. Control. Fusion.*, vol. 31, pp. 147–156, 1989.
[22] A. J. Lichtenberg and M. A. Lieberman, *Regular and Chaotic Dynamics*, 2nd ed. Berlin, Germany: Springer-Verlag, 1992.
[23] A. Vannucci, O. W. Bender, I. L. Caldas, I. C. Nascimento, I. H. Tan, and E. K. Sanada, "Influence of resonant helical windings on the Mirnov oscillations in a small tokamak," *Nuovo Cimento D*, vol. 10, pp. 1193–1198, 1988.
[24] J. M. Finn, "The destruction of magnetic surfaces in tokamaks by current perturbations," *Nucl. Fusion*, vol. 15, p. 845, 1975.
[25] A. S. Fernandes, M. V. A. P. Heller, and I. L. Caldas, "The destruction of magnetic surfaces by resonant helical windings," *Plasma Phys. Control. Fusion*, vol. 30, pp. 1203–1211, Oct. 1988.
[26] L. H. A. Monteiro, V. Okano, M. Y. Kucinski, and I. L. Caldas, "Magnetic structure of toroidal helical fields in tokamaks," *Phys. Lett. A*, vol. 193, pp. 89–93, 1994.
[27] T. J. Martin and J. B. Taylor, "Ergodic behavior in a magnetic limiter," *Plasma Phys. Control. Fusion*, vol. 26, pp. 321–340, 1984.
[28] X. Y. Yu and J. S. DeGrassie, "Mapping techniques for the GA ergodic magnetic limiter experiment on TEXT," Fusion Res. Center, Austin, TX, Univ. Texas Rep. FRC-292, Nov. 1986.
[29] R. L. Viana and D. B. Vasconcelos, "Field-line stochasticity in a tokamak with an ergodic magnetic limiter," *Dyn. Stab. Syst.*, vol. 12, pp. 75–88, Feb. 1997.
[30] R. L. Viana, "Chaotic magnetic field lines in a tokamak with resonant helical windings," *Chaos Solitons Fractals*, vol. 11, pp. 765–778, May 2000.
[31] W. A. Craven, "Resonant external magnetic perturbations in the Texas experimental tokamak," Ph.D. dissertation, Report FRCR-489, Fusion Research Center, University of Texas at Austin, 1996.
[32] A. Boozer and A. B. Rechester, "Effect of magnetic perturbations on divertor scrape-off width," *Phys. Fluids*, vol. 21, pp. 682–680, 1978.
[33] R. Balescu, "Hamiltonian nontwist map for magnetic field lines with locally reversed shear in toroidal geometry," *Phys. Rev. E, Stat. Phys. Plasmas Fluids Relat. Interdiscip. Top.*, vol. 58, p. 3781, Sept. 1998.
[34] M. Y. Kucinski and I. L. Caldas, "Toroidal helical fields," *Z. Naturforsch.*, vol. 42a, pp. 1124–1132, 1987.
[35] W. D. D'haeseleer, W. N. G. Hitchon, J. D. Callen, and J. L. Shohet, *Flux Coordinates and Magnetic Field Structure*. Berlin, Germany: Springer-Verlag, 1991.
[36] M. Y. Kucinski, I. L. Caldas, L. H. A. Monteiro, and V. Okano, "Toroidal plasma equilibrium with arbitrary current distribution," *J. Plasma Phys.*, vol. 44, pp. 303–311, Oct. 1990.
[37] J. D. Jackson, *Classical Electrodynamics*, 2nd ed. New York: Wiley, 1975, pp. 75–78.
[38] A. I. Morozov and L. S. Solov'ev, "The strucutre of magnetic fields," in *Reviews of Plasma Physics*, M. A. Leontovich, Ed. New York: Consultants Bureau, 1966, vol. 2, pp. 1–100.
[39] W. H. Press, S. A. Teukolsky, W. T. Wettering, and B. P. Flannery, *Numerical Recipes in Fortran*, 2nd ed. Cambridge, U.K.: Cambridge Univ. Press, 1992, pp. 718–727.
[40] B. V. Chirikov, "A universal instability of many dimensional oscillator systems," *Phys. Rep.*, vol. 52, pp. 265–379, 1979.
[41] I. L. Caldas, J. M. Pereira, K. Ullmann, and R. L. Viana, "Magnetic field line mappings for a tokamak with ergodic limiters," *Chaos Solitons Fractals.*, vol. 7, pp. 991–1010, July 1996.
[42] R. L. Viana and I. L. Caldas, "Peripheral stochasticity in tokamaks—The Martin–Taylor model revisited," *Z. Naturforsch.*, vol. 47a, pp. 941–944, 1982.
[43] K. Ullmann and I. L. Caldas, "A symplectic mapping for the ergodic magnetic limiter and its dynamical analysis," *Chaos Solitons Fractals*, vol. 11, pp. 2129–2140, Oct. 2000.
[44] S. S. Abdullaev, "A new integration method of Hamiltonian systems by symplectic maps," *J. Phys. A, Math. Gen.*, vol. 32, pp. 2745–2766, Apr. 1999.

[45] E. C. da Silva, I. L. Caldas, and R. L. Viana, "Bifurcations and onset of chaos on the ergodic magnetic limiter mapping," Chaos Solitons Fractals, submitted for publication.
[46] ——, "Field line diffusion and loss in a tokamak with ergodic magnetic limiter," *Phys. Plasmas*, vol. 8, pp. 2855–2865, June 2001.
[47] P. M. Morse and H. Feshbach, *Methods of Theoretical Physics*. New York: McGraw-Hill, 1953, vol. 2.

**Elton César da Silva** was born in 1966. He received the B.S. degree in physics from the University of São Paulo, São Paulo, Brazil, in 1990, and is currently pursuing the Ph.D. degree.

He has been with the Technological Center of the Brazilian Navy in São Paulo for the past six years. His research interests include chaos theory and econophysics.

**Iberê Luiz Caldas** was born in Santos, Brazil, in 1948. He received the B.S. and Ph.D. degrees in physics from the Institute of Physics of University of São Paulo (IF-USP), São Paulo, Brazil, in 1970 and 1979, respectively.

In 1977–1979, 1983, 1984, and 1988, he was a guest scientist at the Max-Planck-Institut fuer PlasmaPhysik (Germany). Since 1995, he has been a Full Professor at IF-USP. His research interests include plasma physics and chaos.

**Ricardo Luiz Viana** received his B.S. degree in physics from the Federal University of Parana, Brazil, and the M.S. and Ph.D. degrees in physics from the University of São Paulo, São Paulo, Brazil in 1985, 1987, and 1991, respectively.

Since 1989, he has been a Professor of Physics at the Federal University of Parana. In 1997, he was a visiting scholar at the University Maryland, College Park. His research interests include the area of chaos applications in plasma physics.